How to Cite: Al-Abbasi, A., Sida, H., Matter, H., & Massoud, F. (2026). Experimental and Theoretical Evaluation of Pentoxifylline as a Sustainable Corrosion Inhibitor for Medium Carbon Steel in HCl. *Eurasian Journal of Chemistry, 31, 3(123), 66–85.* https://doi.org/10.31489/2959-0663/3-26-15

Article

Received: 11 June 2026 | Revised: 18 August 2026 |
Accepted: 24 August 2026 | Published online: 2 September 2026

UDC 544.65:544.18:547.857.4

https://doi.org/10.31489/2959-0663/3-26-15

Aisha Al-Abbasi[1]*, Hussan Sida[2], Hamdy Matter[3], Fatima Massoud[4]

[1]*Chemistry Department, Faculty of Science, Sebha University, Sebha, Libya*
[2]*Scientific Research Consultation Center, Sebha University, Sebha, Libya*
[3]*Chemistry Department, Faculty of Science, Benghazi University, Benghazi, Libya*
[4]*Chemical Engineering Department, Faculty of Engineering, Sebha University, Libya*
(**Corresponding author's e-mail: ais.alabbasi@sebhau.edu.ly*)

Experimental and Theoretical Evaluation of Pentoxifylline as a Sustainable Corrosion Inhibitor for Medium Carbon Steel in HCl

This study aims to evaluate pentoxifylline (PTF), a pharmaceutical drug, as a sustainable green corrosion inhibitor for medium carbon steel in a 0.2 M HCl environment, addressing the critical need for non-toxic industrial alternatives. Experimental investigations were conducted using gravimetric weight loss measurements, hydrogen evolution tests, and electrochemical Tafel polarization across a temperature range of 293.15 to 313.15 K. Theoretical analyses, including Density Functional Theory (DFT) and Monte Carlo simulations, were further employed to explore molecular reactivity and adsorption behavior on the Fe (110) surface. The results revealed that inhibition efficiency increases with PTF concentration, reaching a maximum of 90.0 % at 500 ppm and 293.15 K. Thermodynamic parameters indicated that the process follows the Langmuir isotherm through a spontaneous physical adsorption mechanism. Electrochemical data confirmed that PTF acts as a mixed-type inhibitor, effectively suppressing both anodic metal dissolution and cathodic hydrogen evolution. Furthermore, the addition of iodide ions demonstrated a significant synergistic effect, enhancing the protective capacity to 99.4 %. In conclusion, PTF serves as a highly effective eco-friendly alternative for steel protection. Future research is recommended to investigate the long-term stability of PTF under dynamic industrial flow conditions.

*Keywords: g*reen inhibitor, corrosion inhibitor, adsorption, pentoxifylline, medium carbon steel, HCl, adsorption isotherms, Tafel polarization, Langmuir isotherm, DFT calculations.

1 Introduction

Corrosion is one of the most critical concerns for metal and industrial material. It is caused by a slow chemical or electrochemical reaction between material and the environment [1]. This phenomenon is the root cause of severe erosion in many metallic systems and industries. Rusting can take place on metals, polymers, and even ceramics. In aqueous solutions, corrosion is predominantly a result of electrochemical processes, in different times scale due to electrons exchange between metal surface and electrolyte solution. Corrosion induced economic loss is incredibly colossal and estimated to be trillion dollars on an annual basis across the globe [2, 3]. Apart from economic impact, it can also bring about environmental and health consequences, especially if metal containers are used to hold food, water, or pharmaceutical products.

Steel is the most commonly used material in high pressure industrial application because of its availability at low cost, high mechanical strength and ease of fabrication. They are widely utilized in the oil and gas fields, tank farms, pipelines, heat exchangers and chemical processing plants [4]. On the other hand, steel surfaces are extremely susceptible to corrosion in contact with acidic solutions. Acidic media are widely employed in industrial processes including acid cleaning, pickling, descaling, and oil well acidizing [5]. In this type of system, H^+ and dissolved O_2 are also good corrosion promoters, and they are active in high-temperature water environments. Hence, the steel surface protection in acidic media is still a challenging issue.

Numerous techniques have been evolved to mitigate corrosion damage. Such methods are protective coatings, cathodic protection, anodic protection, and the addition of corrosion inhibitors [6]. Corrosion inhibitors are one of the most feasible and cost-effective methods to combat corrosion, particularly in acidic media, of these methods. Corrosion inhibitors decreases the solubility of metal either by adsorbing at the metal surface forming a film or by modifying electrochemical reactions at the interface [7]. Organic com-

pounds having heteroatoms such as N, O, S and P are reported to have good inhibition properties as these atoms are able to interact with the metal surface by their lone pair of electrons and π-electrons [7-15].

Although a lot of synthetic inhibitors are of high efficiency, some of them are toxic, costly and have environmental hazards. Therefore, due to the toxicity of some of the inhibitors used, recent efforts have been directed towards the synthesis of non-toxic, greener inhibitors. Due to their non-toxic nature and biodegradability, natural products and pharmaceuticals have been widely considered for application as green corrosion inhibitors for metals. Expired drugs are highly promising products since they can be considered as candidates for reuse rather than being disposed as waste [16-19]. Numerous pharmaceutical molecules have aromatic rings and heteroatoms that increase their propensity to adsorb on metal surfaces, and can be investigated for potential use in corrosion inhibition [20, 21]. However, a critical review of the existing literature reveals a significant gap in the detailed atomistic understanding of how hexadentate drug molecules like Pentoxifylline interact with the Fe (110) surface, particularly when combined with inorganic synergistic ions in HCl media. Most existing studies focus on macroscopic experimental observations without providing a rigorous theoretical correlation to justify their industrial efficacy.

To address these limitations, the present study offers a novel, multi-faceted evaluation that bridges the gap between experimental performance and theoretical molecular dynamics. In this investigation, hexadentate pentoxifylline (PTF) was adopted as the inhibitor for the corrosion of medium carbon steel in 0.2 M HCl. The adsorption and inhibition properties of PTF were investigated through weight loss studies, hydrogen evolution, electrochemical methods and quantum chemical calculations. Moreover, the effect of iodide ions as synergist on the inhibitive performance of PTF was also investigated. The novelty and scientific contribution of this work lie in the precise integration of high-level Density Functional Theory (DFT) and Monte Carlo simulations on the Fe (110) surface to elucidate the electronic donor-acceptor mechanisms of PTF, providing new insights into sustainable and highly efficient multi-component corrosion protection systems that have not been fully explored in previous literature.

2 Experimental

2.1 Materials

Pentoxifylline (400 mg tablets) was a gift from Santa Farma, Turkey. The medium carbon steel samples were procured from Libyan Steel Factory, Libya. Elemental composition of the steel was C (0.33 %), Si (0.17 %), Mn (0.72 %), P (0.013 %), S (0.002 %), and Fe (98.765 %). For the weight loss test, the steel was cut mechanically into cylindrical pieces having the dimensions of 4 cm in length and 1 cm in diameter. Surface were polished with SiC abrasive papers (400–1200 grit size). After polishing, the test samples were rinsed with ethanol and acetone, air-dried and kept in desiccators to protect from moisture prior to utilization. A stock solution of hydrochloric acid (5.0 N) was prepared from commercial HCl (37 %) and standardized against sodium carbonate solution. The necessary concentration of 0.2 M HCl was prepared by dilution with deionized water. A stock solution of pentoxifylline inhibitor (1000 ppm) was prepared and the various concentrations viz., 50 to 500 ppm were tested in the study.

2.2 Instrumentation

The experimental procedures, including gravimetric measurements and hydrogen evolution tests, were conducted at the Chemistry Department, Faculty of Science, Sebha University, Libya. The weight loss experiments were performed using a precision analytical balance (Ohaus, Ga110-Made in West Germany). A thermostatic water bath to maintain constant temperatures (Clifton Bata-England). Electrochemical measurements, including potentiodynamic Tafel polarization, were carried out using a Potentiostat, manufactured by ACM Instruments (field model). The medium carbon steel was sourced from the Libyan Steel Factory, Libya. For the computational modeling, Density Functional Theory (DFT) and Monte Carlo simulations were executed at the Scientific Research Consultation Center, Sebha University, using the BIOVIA Materials Studio software (version 5.5) developed by Accelrys (now BIOVIA, USA).

2.3 Gravimetric Estimations

For the weight loss test, the steel was precisely cut into cylindrical pieces (4 cm length, 1 cm diameter) using a lathe machine. The cutting process was performed under continuous liquid cooling to prevent thermal overheating and minimize mechanical induced stresses on the steel specimens. This ensures that the metallurgical properties of the medium carbon steel remain unchanged during preparation. Subsequently, the surfaces were polished with SiC abrasive papers (400–1200 grit size) to remove any residual surface irregularities. After polishing, the test samples were rinsed with ethanol and acetone, air-dried and kept in desicca-

tors to protect from moisture prior to utilization. The pre-weighed medium carbon steel samples were fully immersed in 50 mL of various concentrations of inhibitors from 50 to 500 ppm. The tests were performed in a thermostatically water bath at various temperatures. At the end of the Soaking time, the steel samples were taken out, cleaned and dried then weighed once more. The values of weight loss were calculated by subtracting the final weight of the samples from the initial weight. Each experiment was performed in triplicate for reproducibility. Corrosion rate (CR) in mmy is calculated using Equation (1) [22, 23]:

$$\mathrm{CR}\left(\mathrm{mmy}\right) = \frac{8.76\times10^{4}W}{\mathrm{At}D} \tag{1}$$

From the corrosion rate data, the inhibition efficiency (% Inh) and the surface coverage (θ) were calculated with help of the following equations (2) and (3).

$$I\% = \left(1 - \frac{CR_{inh}}{CR_0}\right)\times100 \tag{2}$$

$$\theta = \left(1 - \frac{CR_{inh}}{CR_0}\right) \tag{3}$$

where CR_0 is the corrosion rate without and CR_{inh} is the corrosion rate with the inhibitor.

2.4 Hydrogen Evolution Tests

Hydrogen evolution experiments were carried out in a closed flask assembled to an inverted burette via a plastic tube [24]. The flask was filled with 0.2 M HCl solution, PTF inhibitor was also therein, as well as none. The system was kept at 303.15 K by a thermostatic water bath. The volume of released hydrogen gas was recorded every 2 min for 60 min. The experiments were performed with and without 200ppm PTF as well as iodide ion as a synergistic additive. Hydrogen evolution rate (Hr) was calculated using Equation (4).

$$\mathrm{H_r} = \left(\mathrm{V_2} - \mathrm{V_1}\right)/\left(\mathrm{t_2} - \mathrm{t_1}\right) \tag{4}$$

where V_1 and V_2 are the volumes of hydrogen observed at times t_1 and t_2, respectively. The volume of hydrogen was plotted against the immersion time, and the slope of the resulted straight line was the corrosion rate. The inhibition efficiency was calculated from the Equation (5) [25]:

$$\mathrm{Inh\%} = \left[1\left(H_0 / \mathrm{H}_{inh}\right)\right]\times100 \tag{5}$$

where H_0 and Hinh are the rates of hydrogen evolution in the absence and presence of inhibitor respectively.

2.5 Tafel Polarization Tests

The electrochemical cell contained a working electrode– a suitable electrode for the solution being studied, Ag/AgCl reference electrode, and carbon rod as counter electrode. The potentiodynamic polarization experiments were performed by sweeping the potential from −500 mV versus the open circuit potential (OCP) to +500 mV vs. OCP at a scan rate of 1 $\mathrm{mVs^{-1}}$. The working electrode was made by insulating all sides but one exposed face joined by a copper wire. Prior to each run, the surface of the steel was polished with different sized abrasive papers (60-1200 grit). The measurements were made at room temperature with a 1000 mL capacity open electrochemical cell in 0.2 M HCl solution with and without 500 ppm of PTF inhibitor.

2.6. Computational Details

2.6.1. Molecular Reactivity and Molecular Dynamics

The density functional theory calculations were carried out with Materials Studio software via the $\mathrm{DMol^3}$ module (version 5.5). To ensure scientific validity and reproducibility, all calculations were performed using the Double Numerical plus Polarization (DNP) basis set. The calculations were conducted in the gas phase to investigate the intrinsic molecular reactivity of PTF, following the standard methodology widely adopted in established corrosion inhibition research. This approach ensures that the electronic descriptors (HOMO, LUMO, etc.) represent the inherent donor-acceptor capacity of the molecule without the shielding effects of a dielectric medium, allowing for direct comparison with literature data. Geometry optimizations were carried out with high-precision convergence criteria (1.0×10^{-5} Ha for energy and 0.002 Ha/Å for force) to ensure that the stationary structures represent true energy minima, consistent with stable configurations reported in previous studies using similar functionals. calculations were performed at the level of the generalized gradient approximation (GGA) within the BLYP exchange correlation functional [26, 27].

The frontier molecular orbitals, HOMO and LUMO, are also considered in order to study the adsorption characteristics of the organic compounds on the metal surface. Based on Koopman's theorem, the HOMO and the LUMO energies were utilized to calculate the values of the ionization potential and the electron affinity [28-30].

$$\Delta E = E_{LUMO} - E_{HOMO} \quad (6)$$

$$I = -E_{HOMO} \quad (7)$$

$$A = -E_{LUMO} \quad (8)$$

Other quantum chemical descriptors like electronegativity (χ), hardness (η), and softness (σ) of the inhibitor molecule are given by Pearson [30].

$$\chi = \frac{I + A}{2} \quad (9)$$

$$\eta = \frac{I - A}{2} \quad (10)$$

$$\sigma = \frac{1}{\eta} \quad (11)$$

The fraction of electrons transferred (ΔN), and electrophilicity index (ω) were also derived as follows [31]:

$$\Delta N = \frac{\chi_{Fe} - \chi_{inh}}{2(\eta_{Fe} + \eta_{inh})} \quad (12)$$

Using a theoretical value, $\chi_{Fe} = 7eV$ and the value of $\eta_{Fe} = 0$ eV for iron according to Pearson's electronegativity scale[22]. The electrophilicity index (ω) has been defined as [32-34]:

$$\Delta\omega = \frac{\chi^2}{2\eta} \quad (13)$$

2.6.2 Monte Carlo Simulations

Monte Carlo simulations were carried out to study the adsorption of PTF molecules on Fe (110) surface using the Adsorption Locator module within the Materials Studio software package, as it is specifically designed for identifying low-energy adsorption configurations. The Forcite module was utilized only for the initial geometry optimization of the inhibitor and the metal surface. The calculations were performed with the COMPASS force field (Condensed-phase Optimized Molecular Potentials for Atomistic Simulation Studies) [35, 36]. The Fe surface was cut along the (110) plane and modeled as a supercell with dimensions of 12 Å × 12 Å, which provides sufficient surface area to host a single PTF molecule while minimizing periodic self-interaction artifacts. A vacuum thickness of 15 Å was used to suppress the spurious interactions between periodic images along the z-axis. While the simulations were conducted in a vacuum to establish a fundamental baseline for the intrinsic binding energy, this gas-phase approximation effectively identifies the preferred molecular orientation on the iron lattice. The adsorption search was performed using the Metropolis Monte Carlo algorithm within the NVT statistical ensemble (constant number of particles, volume, and temperature) at 298.15 K. The simulation consisted of a total of 1,000,000 Monte Carlo steps, including 100,000 equilibration cycles followed by 900,000 production/sampling cycles to sample the identification of the global energy minimum. For non-bonded interactions, a cutoff distance of 12.5 Å was applied, utilizing the Ewald summation method for electrostatic interactions and the atom-based method for van der Waals interactions.

3 Results and Discussion

3.1 Mass Loss Approach

3.1.1 The Inhibition Properties of Pentoxifylline Drugs

The Inhibition Properties of Pentoxifylline Drugs Table 1 and Figure 1 illustrate the results for the estimated corrosion rate (mmy) and inhibition efficiency (Inh%) of medium carbon steel in 0.2 M HCl solution in the presence and absence of various doses of PTF inhibitor (100–500 ppm). The results demonstrate that the corrosion rate of medium carbon steel was significantly reduced after the addition of PTF compared with that in the blank solution. As shown in Figure 1, the corrosion rates decreased stepwise with increasing in-

hibitor concentration. This behavior implies that PTF molecules successfully inhibit the dissolution of steel in HCl medium through adsorption onto the steel surface [37].

Table 1

Corrosion rates (C.R., mmy) for HCl (0.2 M) induced medium carbon steel dissolution with and without inhibitor at different temperatures.

Inhibitor Conc., ppm	293.15 k		303.15 k		313.15 k	
	C.R., mmy	Inh., %	C.R., mmy	Inh., %	C.R., mmy	Inh., %
0	11.416	-	21.2600	-	59.682	-
100	2.7366	76.0278	6.1120	71.2512	7.466	43.1941
200	1.7693	84.5011	4.8609	77.1357	5.135	62.7341
300	1.5292	86.6039	4.4890	78.8851	4.461	67.7512
400	1.1824	89.6426	3.5538	83.2840	4.21	69.0759
500	1.1404	90.0099	3.1573	85.1492	5.515	69.6574

The data presented in Table 1 also indicates that temperature has a positive impact on the rate of corrosion. The efficiency of inhibition became less at several temperatures ranging between 293.15 and 313.15 K. This may be due to the fact that the corrosion reaction was accelerated under high temperature. Moreover, the rise in temperature might result in the desorption of PTF from the steel surface and disclosure of more metal atoms to the acidic solution by destruction of the protective layer. The maximum inhibition efficiency achieved by PTF (90.0 %) is notably higher than the 84.9 % efficiency reported by Popović for expired metformin, suggesting that PTF's hexadentate structure provides more extensive surface coverage on the steel substrate [38].

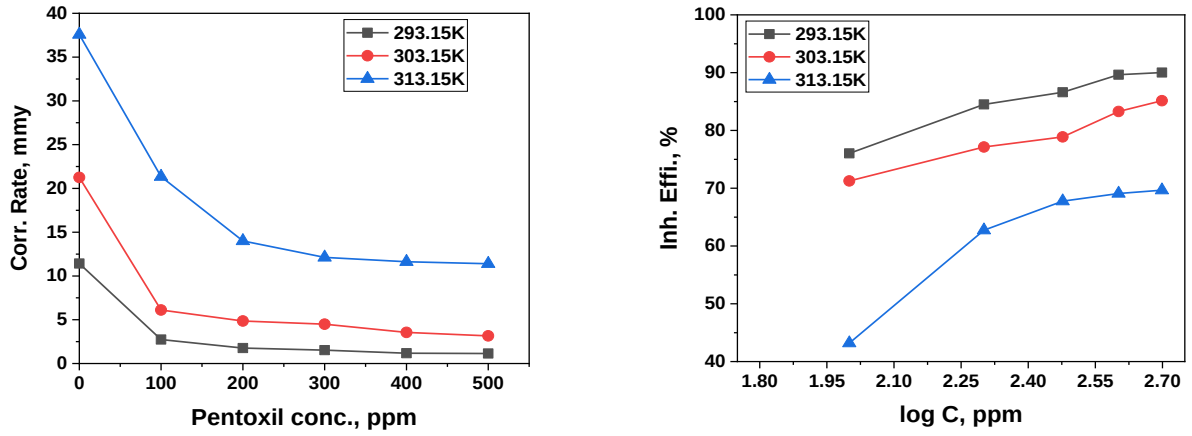

Figure 1. Corrosion rate (A) and inhibition efficiency (B) of PTF at different concentrations

3.1.2 Thermodynamic Parameters of the Corrosion Inhibition

Figure 2 presents the inhibition efficiency of PTF on the medium carbon steel surface as a function of changing temperature. The results show that the inhibition efficiency decreased with the temperature, indicating that the protective film of PTF molecules is unstable at high temperatures [39]. In contrast to the findings of Mahmood, where inhibition efficiency showed a slight increase with temperature, PTF exhibits a decrease, which confirms the predominantly physical nature of its adsorption compared to the chemisorptive behavior of p-bromopiperazinylbenzene [40].

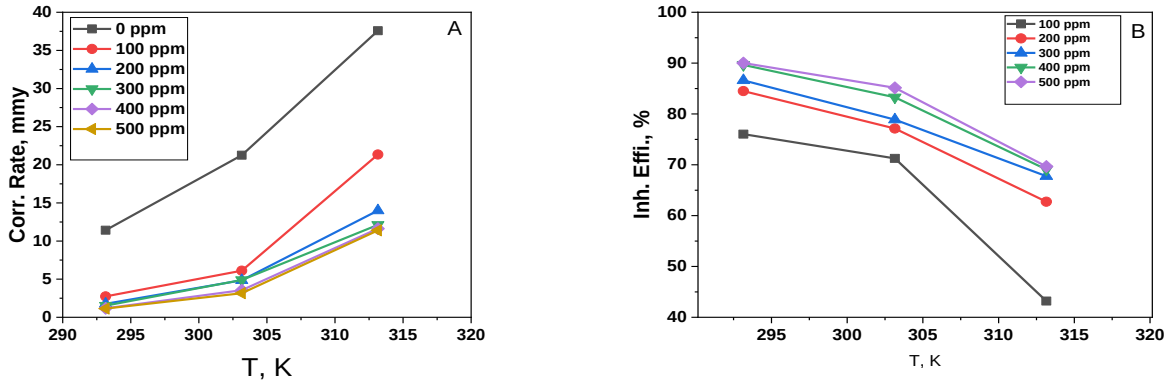

Figure 2. Corrosion rate (A), and efficiency of inhibition (B), at different temperatures

The activation parameters of the corrosion are needed to better understanding the mechanism of inhibition. The temperature dependence of the corrosion rate was analyzed in terms of the Arrhenius equation [41-43]:

$$\ln R = \ln A - \frac{\Delta E_a^*}{\mathcal{R}T} \quad (14)$$

where R is the universal gas constant, ΔE_a^* is the apparent activation energy and A is the Arrhenius pre-exponential factor. The Arrhenius plots are given in Figure 3. In all plots, perfect or close to unity, (R^2: 0.998-1.000), liner Arrhenius behaviour was confirmed. Energy of activation calculations and are said to be derived from the slopes of these plots. Thermodynamic parameters were also calculated through the transition-state equation [43-45]:

$$\ln\left(\frac{R}{T}\right) = \left[\ln\frac{\mathcal{R}}{N^O h} + \frac{\Delta S_a^*}{\mathcal{R}}\right] - \frac{\Delta H_a^*}{\mathcal{R}T} \quad (15)$$

where h is Planck's constant, N is Avogadro's number, ΔS_a^* is the activation entropy and ΔH_a^* a is the activation enthalpy. The changes in free energy of activation for thermal decomposition, ΔG_a^*, were also determined. The values of enthalpy of activation ($\sqrt{\Delta H_a^*}$) and entropy of activation ($\sqrt{\Delta S_a^*}$), which are shown in Table 2, were calculated using the slope and intercept of the curves.

$$\Delta G_a^* = \Delta H_a^* - T\Delta S_a^* \quad (16)$$

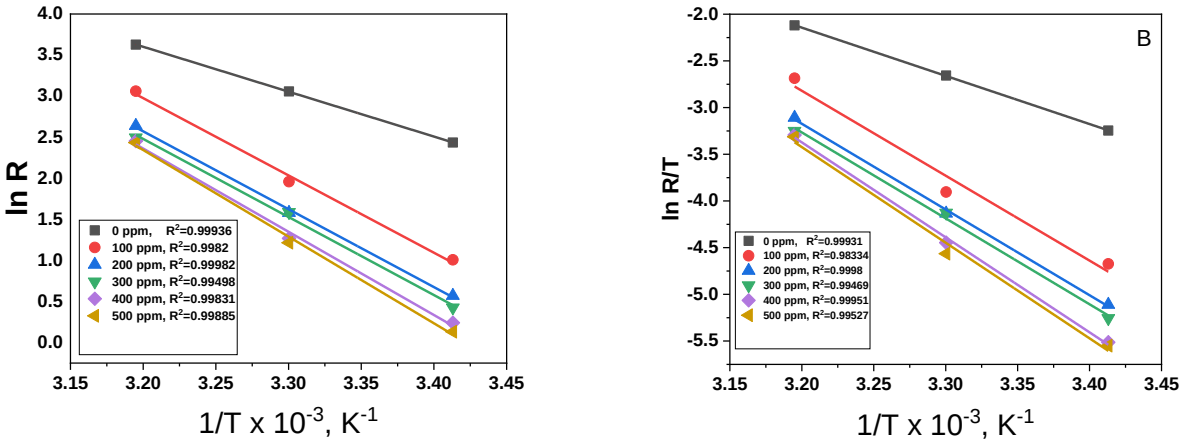

Figure 3. Arrhenius (A) and transition state (B) plots for the corrosion of medium carbon steel in 0.2 M HCl in the absence and presence of PTF

Table 2 provides the calculated thermodynamic parameters, including the activation energy (ΔE_a^*), enthalpy (ΔH_a^*), and entropy ΔS_a^*, which were derived from the Arrhenius and transition-state plots shown in Figure 3 [46-48].

Table 2

Values of the thermodynamic constants for the dissolution of medium carbon steel in the absence and presence of PTF in 0.2 M HCl

Inhibitor Conc., ppm	ΔE_a^*, KJ·mol^{-1}	ΔH_a^*, KJ·mol^{-1}	ΔS_a^*, J·mol^{-1}K^{-1}	ΔG_a^*, KJ·mol^{-1}		
				293.15, K	303.15, K	313.15, K
0	45.477	42.958	-77.969	65.815	66.594	67.374
100	78.178	75.66	21.001	69.504	69.294	69.084
200	78.902	76.383	20.378	70.409	70.206	70.002
300	79.004	76.486	19.696	70.712	70.515	70.318
400	87.147	84.628	45.087	71.411	70.960	70.509
500	87.721	85.202	46.525	71.563	71.098	70.633

The thermodynamic shown in Table 2 indicated that all energies of activation were positive, which is evidence of corrosion process endothermic nature. The activation energy was raised in the presence of the inhibitor as compared to the blank solution, denoting that the inhibitor forms a barrier through those acts as the energy barrier that hinders the dissolution of steel. The increase in active energy also implies that inhibition effectiveness may reduce at higher temperatures due to less adsorption of inhibitor molecules onto surface of medium carbon steel [43].

The enthalpy values, Table 2, were found to increase with the concentration of inhibitor. The positive enthalpy values suggest that the inhibition is an endothermic process and the dissolution of steel is more retarded in the presence of high concentrations of PTF [43, 44]. In contrast, after addition of the inhibitor, the entropy values were more negative. This behavior indicates that the activated complex in the corrosion reaction is more ordered than the reactants [21]. The calculated ΔG_a^* values are also presented in Table 2. Positive value was obtained for the blank solution, while negative values were found for the inhibited systems. The increase in value showed that the inhibition reaction is feasible and the transition state became stable as temperature increased [39]. Moreover, the free energy of activation decreased with increasing inhibitor concentration from 50 to 200 ppm, which could be related to the development of the activated complex too being less stable. But, the value of the free energy increased again at 300 — 400 ppm, which was attributed to the generation of a more stable activated complex on the surface of steel [39]. The observed increase in activation energy (ΔE_a^*) upon the addition of PTF (from 45.4 to 87.7 kJ/mol) is consistent with the findings of Malki, who reported a similar upward trend in ΔE_a^* values (from 21.0 to 40.46 kJ/mol), confirming the formation of a physical barrier that restricts the corrosion process [49].

3.1.3 Synergistic Effect

Table 3 and Figure 4 present the corrosion rate and inhibition efficiency values at 303.15 K, demonstrating the synergistic effect between iodide ions and PTF molecules [27 ،28]. Furthermore, Table 4 and Figure 5 show the impact of fixed potassium iodide (KI) concentration on the inhibitory performance of varying PTF concentrations [29 ،30]. The S_I values in these tables indicate strong synergistic behavior between iodide ions and PTF molecules.

Table 3

Corrosion rate and inhibition efficiency at 303 K in the presence of KI and PTF

KI conc., ppm	0, ppm PTF		200, ppm PTF		
	C.R., mmy	Inh, %	C.R., mmy	Inh, %	SI
0	21.260	-	4.861	77.136	-
50	17.626	17.094	2.069	90.269	1.948
100	15.773	25.811	1.934	90.903	1.865
150	14.310	32.693	1.869	91.210	1.751
200	12.617	40.655	1.620	92.380	1.781

The inhibition efficiency increased dramatically with the addition of iodide ions as shown in Table 3. The maximum protection was achieved at 200 ppm KI with inhibition efficiency 92.38 % in presence of 200 ppm PTF. The decrease in the corrosion rate proves the presence of a synergistic effect between iodide ions and PTF molecules. This can be related to the fact that the iodide ions can promote the steel surface adsorption of inhibitor molecules. Iodide ions are much more strongly adsorbed due to their big ionic size and high polarizability. Their adsorption promotes the interaction of PTF molecules with the metal surface, so that a denser protective film is formed [50, 51]. Our synergistic PTF/Iodide system (99.4 %) demonstrates superior performance compared to the dual-inhibitor compositions evaluated by Tsygankova, such as the Drotaverine/KCNS mixture which reached 98.0 % efficiency [52].

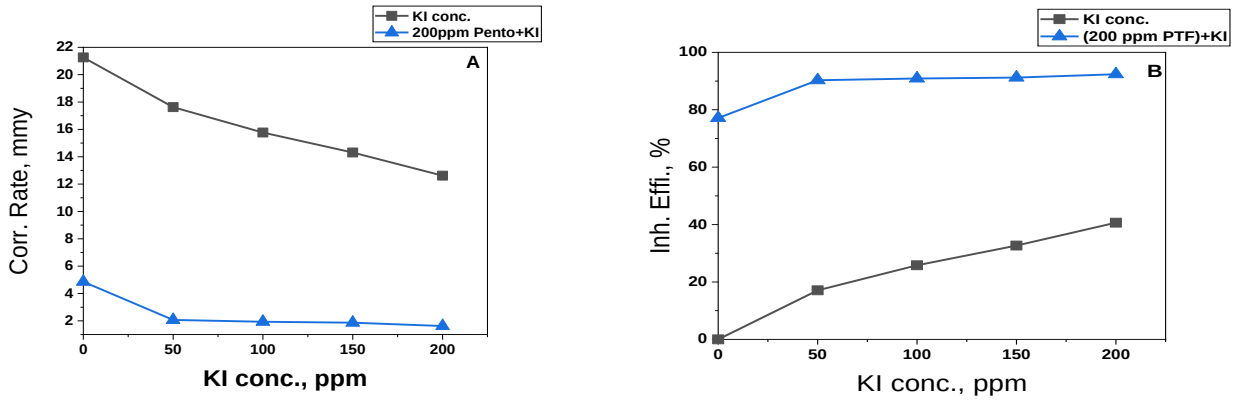

Figure 4. Corrosion rate (A) and inhibition efficiency (B) as a function of KI concentration in the presence of PTF at 303.15 K

These findings also reveal that the corrosion rate continuously decreases with raising KI content. Under dual PTF and KI presence the rate of corrosion was even lower than that in the solutions containing only potassium iodide. This is attributed to the fact that progressively adsorption of PTF molecules enhances the coverage and protective oil film on the steel substrate. Similarly, the inhibition efficiency increased as the KI concentration increased. Furthermore, the inhibitory effectiveness in the binary system of KI + PTF was superior to that of PTF alone, indicating a synergistic positive effect of the iodide ions. A concentration of KI of 150 ppm was chosen to investigate more the inhibition performance of the medium carbon steel in acidic medium containing variable concentrations of PTF at fixed KI concentration. The corrosion rates and subsequent inhibitor efficiencies calculated are presented in Table 4 and Figure 5.

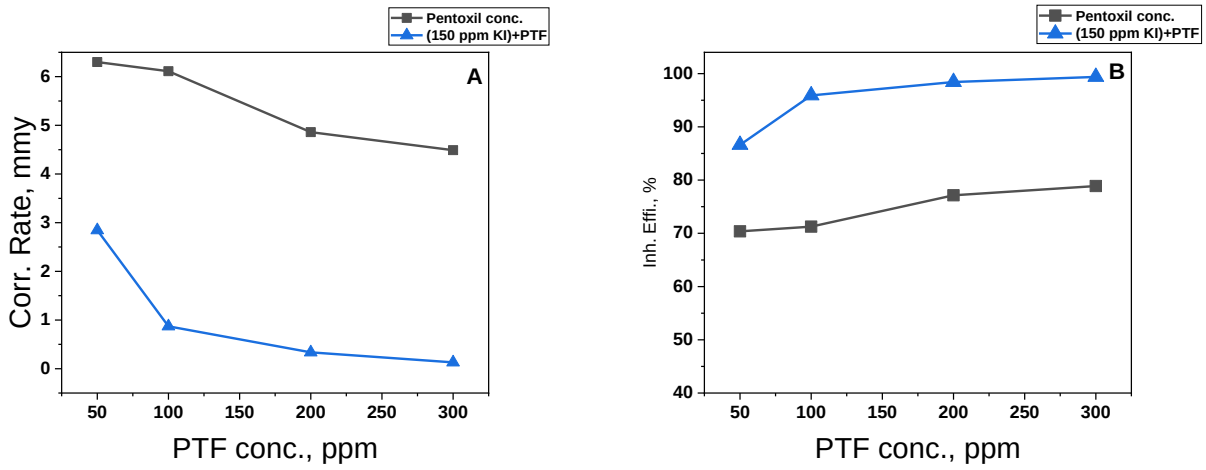

Figure 5. Corrosion rate and inhibition efficiency in the presence of PTF, with a fixed concentration of KI at 303.15 K

Table 4

Corrosion rate and inhibition efficiency in the presence of PTF, with a fixed concentration of KI at 303.15 K

PTF conc., ppm	0, ppm KI		150, ppm KI		
	C.R., mmy	Inh, %	C.R., mmy	Inh, %	SI
50 ppm	6.300	70.367	2.846	86.614	1.490
100 ppm	6.112	71.251	0.871	95.902	4.721
200 ppm	4.861	77.136	0.337	98.416	9.715
300 ppm	4.489	78.885	0.130	99.387	23.169

In acidic medium, the corrosion of steel surface produces positively charged metal ions [51]. In these circumstances, PTF molecules may be adsorbed on the steel surface [53-55]. Meanwhile, iodide ions can also be readily adsorbed by electrostatic attraction since it is negatively charged and the metallic cation are positively charged [51]. Iodide ion adsorption decreases the rate of corrosion and the number of delocalized active sites on the surface of steel. Iodide ions significantly enhance the adsorption of PTF molecules on the steel surface and assist in the formation of a strong anti-corrosive film on steel. When the KI concentration was about 150 ppm, the co-adsorption process was the most effective with an inhibition efficiency of 99.3866 % in the presence of 300 ppm PTF.

The synergism influence between PTF and iodide ions was estimated by the synergistic parameter (SI), which is defined as follows [57-55]:

$$SI = \left(1 - I_{1+2}\right) / \left(1 - I'_{1+2}\right) \quad (18)$$

Here I_1 and I_2 are the inhibition efficiency of iodide ions and PTF respectively, and I'_{1+2} is the inhibition efficiency for the presence of KI and PTF together. Interpretation The S_I values indicate synergistic effects for values exceeding unity in the reverse for less than unity [51, 58, 59]. The case with iodide ions and PTF also has the highest values of S_I listed in Tables 3 and 4, indicating very strong synergistic behaviour between iodide ions and PTF molecules in that particular situation.

3.1.4 Adsorption Isotherms

Figure 6 displays the linearity of the experimental values fitted to the Langmuir, El-Awady, Temkin, and Freundlich adsorption isotherm models. Table 5 lists the calculated adsorption parameters, including the equilibrium constant (K_{ads}) and the standard free energy of adsorption (ΔG^{o}_{ads}), derived from these models.

In general, adsorption of organic molecules on a metal surface is the process where already adsorbed water molecules on the steel surface are displaced by the organic molecules in the solution phase. Inhibitor molecules must interact intensely with the metal surface for the adsorption to be successful. These interactions can be of an electrostatic nature and/or by a covalent bonding between the chemisorbed species and the metal surface atoms. Hence, to achieve a better approximation to the adsorption behaviour of the PTF molecule on the medium carbon steel, we considered in this study a number of different adsorption isotherm models. The surface coverage (θ) values obtained from the mass loss technique were used in this analysis. Langmuir, El-Awady, Temkin and Freundlich adsorption isotherms were investigated and thermodynamic parameters of adsorption were calculated, too.

From the examined adsorption models, the Langmuir adsorption model was the most appropriate for the experimental data with the highest values of correlation coefficient (R^2). The Langmuir adsorption model was tested by plotting C/θ as a function of the inhibitor concentration (C), and the data are shown in Figure 6.

$$\frac{C}{\theta} = \frac{1}{K_{ads}} + C \quad (19)$$

where K_{ads} is the equilibrium constant for adsorption. Straight lines with slopes close to unity and the intercepts were $1/K_{ads}$ at all the temperatures studied. The lines high linearity suggest that the PTF molecules on medium carbon steel surface have been the Langmuir isotherm. The values of K_{ads} and ΔG_{ads} calculated are given in Table 5.

Also, the El-Awady isotherm of adsorption was tested by applying Eq. (20). Linear relationships were obtained when $\log(\theta/1-\theta)$ was plotted versus log C as shown in Figure 6. The values of the correlation R^2 were good indicating that fitting of the experimental data were acceptable. The calculated y, 1/y, K_{ads}, and ΔG_{ads} values are reported in Table 5.

$$\log\frac{\theta}{1-\theta} = \frac{1}{y}\log K_{ads} + y\log C \tag{19}$$

The linearized version of the Freundlich equation was used to analyses the adsorption isotherm Freundlich isotherm was also verified by applying the equation in linearized form. Straight lines were obtained when we plot log θ against log C. Their slopes and intercepts are 1/n and log K_{ads}, respectively.

$$\log\theta = \log K_{ads} + \frac{1}{n}\log C \tag{20}$$

The parameter n is an empirical parameter that is related to adsorption properties. In general, as 1/n was between 0 and 1, adsorption process is favorable, when n is near to or less than unity, then the adsorption is unfavorable [60]. The Temkin adsorption isotherm was further employed by Eq. (22). The plots of θ against ln C were linear (Fig 6). The slope and intercept were equal to 1/ *f* and (1/ *f* ln K_{ads}), respectively.

$$\theta = \frac{1}{f}\ln c + \frac{1}{f}\ln K_{ads} \tag{22}$$

The standard free energy of adsorption was determined by the following equation (23) [61]:

$$\Delta G^{o}_{ads} = RT\ln\left(55.5\,K_{ads}\right) \tag{24}$$

where R is the gas constant, T is the absolute temperature and 55.5 is the molar concentration of water in solution. The determined adsorption parameters are listed in Table 5 [37].

The adsorption details for the PTF inhibition of medium carbon steel corrosion in HCl solution are given in Table 5. The values of correlation coefficients for all models were found to be high (R^2 > 0.90), indicating that the experimental data were well fitted by all investigated adsorption models. The superior fit of the Langmuir isotherm (R^2 = 0.999) for PTF adsorption is in full agreement with recent studies by Malki and Abdel-Hameed [49], validating the formation of a stable, protective monolayer of pharmaceutical molecules on the steel surface. However, the Langmuir adsorption isotherm achieved the maximum R^2 values that were close to 0.999 and confirmed that this isotherm best represents the adsorption of PTF molecules on the surface of the medium carbon steel in the medium of hydrochloric acid. The calculated K_{ads} values for the process under study were less than unity, indicating that the adsorption is predominantly physical and that that the PTF molecules and the steel surface are associated via physical forces [37]. This behaviour is very favourable for a protective adsorbed layer formation via electrostatic interaction.

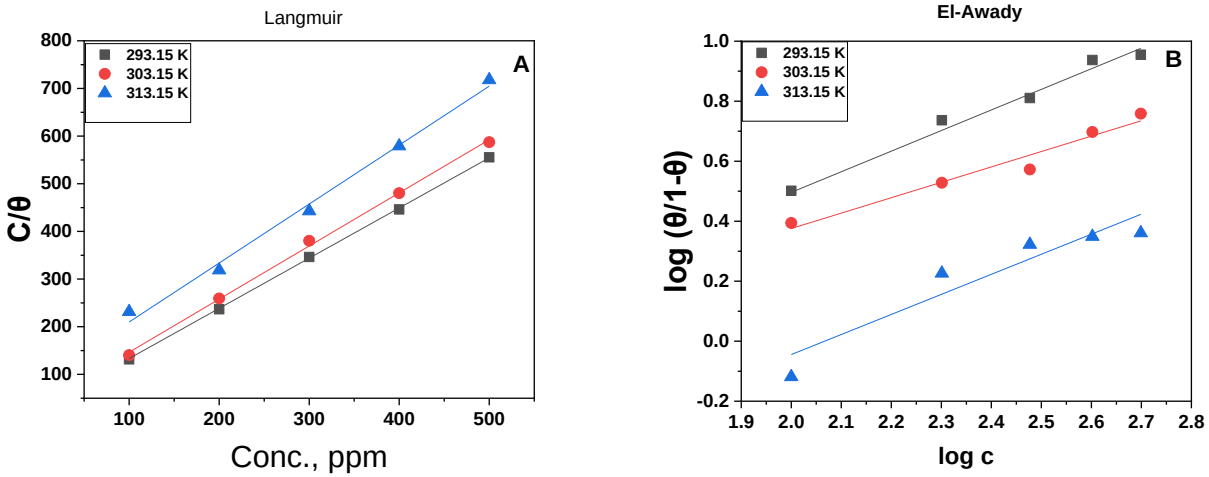

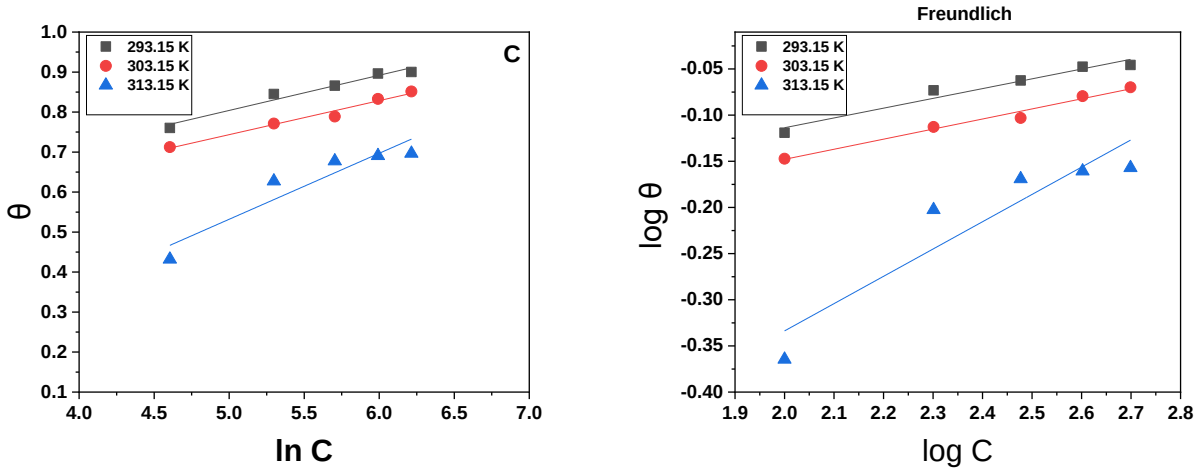

Figure 6. Linearity of the experimental values to the Langmuir (A), El-Awady (B), Temkin (C) and Freundlich (D) fractional productivity adsorption isotherm

Table 5

Adsorption parameters(K_{ads} and ΔG_{ads}) from Langmuir El-Awady and Freundlich isotherm curves at 298 K

	Parameters	293.15, K	303.15, K	313.15, K
Langmuir	K_{ads}	0.038	0.0285	0.0113
	$\Delta G_{ads,}$ KJ·mol^{-1}	-1.908	-1.157	-1.166
Freundlich	K_{ads}	0.473	0.430	0.119
	$\Delta G_{ads,}$ KJ·mol^{-1}	-20.575	-19.549	-5.649
	1/n	0.1059	0.1092	0.2957
El-Awady	K_{ads}	0.155	0.229	0.036
	$\Delta G_{ads,}$ KJ·mol^{-1}	-5.245	-6.408	-1.281
	1/y	1.512	1.964	1.448
	y	0.661	0.509	0.691
Temkin	K_{ads}	63.209	42.093	0.170
	$\Delta G_{ads,}$ KJ·mol^{-1}	-19.893	-19.547	-5.837
	f	11.377	11.751	-6.061
	α	-5.688	-5.875	-3.030

The Temkin adsorption curves for the linear behavior are shown in Figure 6, which reveals that Temkin isotherm can also be used to represent the PTF adsorption. The negative values of α and f imply that attractive interactions exist between the adsorbed PTF molecules on the steel surface.

The El-Awady adsorption model fitting is also shown in Figure 6 and the derived values of y and 1/y are presented in Table 5. The resulting 1/y values imply that a singe PTF molecule covers two active sites on the medium carbon steel surface, which in turn leads to effective surface coverage and enhanced inhibition performance.

The Freundlich adsorption curves are depicted in Figure 6. The calculated 1/n- values fulfil the criteria $0 < 1/n < 1$ which indicates that PTF molecules easily adsorbs on the RS surface [62].

The ΔG_{ads} values calculated at various T are also given in Table 5. The PTF adsorption free energy ΔG_{ads} were all negative and less than −40 kJ/mol, which implied adsorption of the PTF molecules were spontaneous. These findings also confirm that PTF molecules have been adsorbed on the metal surface by electrostatic force between the inhibitor molecules and metal surface, which means that the inhibition process is dominantly governed by physisorption [37].

3.2. Hydrogen Evolution Measurements

Figure 7 illustrates the volume of evolved hydrogen gas as a function of immersion time for medium carbon steel dissolution in 0.2 M HCl, comparing the blank solution with those containing PTF and potassium iodide. Table 6 summarizes the corrosion rates and inhibition efficiencies calculated from these hydrogen evolution measurements.

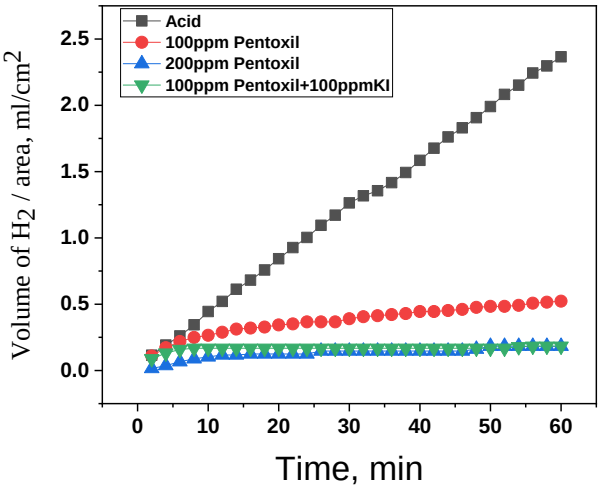

Figure 7. Volume of evolved hydrogen as a function of time for medium carbon steel dissolution in in 0. 2 M HCl with and without PTF and potassium iodide

The volume of evolved hydrogen gas was found to be increased continuously with the increase of immersion time. This is known since hydrogen evolution is a by-product of the corrosion reaction in the acid solution. The hydrogen evolution rate, however, showed an evident decrease when PTF molecules were introduced. The results obtained suggest that a rise in the concentration of PTF is inversely proportional to the amount of produced hydrogen gas. This decrease indicates the surface coverage, and all the above data confirms that I inhibits the corrosion process via adsorption onto the steel surface. Adsorbed inhibitor molecules can create a protective film at the interface of metal and acidic solution that protects the metal from corrosion and also restricts the hydrogen evolution rate. Inhibition efficiency values, based on hydrogen evolution measurement, are presented in Table 6.

Table 6

Corrosion rate and inhibition efficiency of PTFs from hydrogen evolution

Solutions	C.R., $mL \cdot cm^{-2} \cdot min^{-1}$	Inh, %
Acid conc., 0.2, M	0.0388	0
100, ppm PTF	0.0057	85.3093
200, ppm PTF	0.0021	94.5876
100, ppm PTF + 100, ppm KI	0.0005	98.5689

The results showed a continuous increase in the volume of evolved hydrogen gas with increasing immersion time. This behaviour is expected because hydrogen evolution accompanies the corrosion reaction in acidic solution. However, the hydrogen evolution rate decreased noticeably after the addition of PTF molecules. The obtained data indicate that increasing PTF concentration reduces the amount of generated hydrogen gas. This reduction confirms that the inhibitor suppresses the corrosion reaction through adsorption on the steel surface. The adsorbed inhibitor molecules form a protective layer that isolates the metal from the acidic environment and decreases the rate of hydrogen evolution. The marked reduction in hydrogen evolution observed with PTF aligns with the results of Tsygankova, who demonstrated that expired pharmaceutical molecules successfully retard the cathodic hydrogen gas generation in acidic media [52].

PTF molecules adsorb on the surface of the medium carbon steel at the metal/solution interface, inhibiting the dissolution of the steel in HCl solution and hence decreasing the cathodic hydrogen evolution reaction [25]. The inhibitor's molecular structure and its capacity to adsorb on the steel surface are directly associated with the inhibitory properties. Furthermore, the results reveal that the corrosion rate is decreased remarkably in the dual action of PTF and potassium iodide. Inhibitor molecules are adsorbed on the steel surface and organized to serve as a thin, protective layer, which significantly inhibit metal dissolution and hydrogen production.

3.3. Electrochemical Tafel Polarization Tests

Electrochemical polarization studies were conducted to determine the efficiency of PTF as an inhibitor and to gain further insights into the mechanism of inhibition and the durability of the adsorbed inhibitor film on the medium carbon steel surface for an extended time of 22 h immersion. Figure 8 shows the potentiodynamic polarization curves of the medium carbon steel in 0.2 M HCl with and without 500 ppm of PTF inhibitor. As observed in the Figure, the curves with and without the inhibitor appear closely aligned, reflecting the moderate nature of the inhibition effect under these conditions.

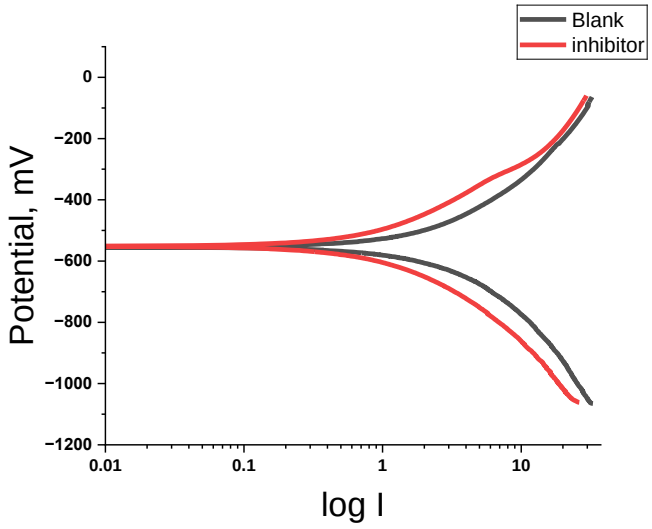

Figure 8. Potodynamical polarization curves of the medium carbon steel in 0.2 M HCl with and without PTF inhibitor

The electrochemical parameters derived from these curves, including corrosion current density (*Icorr*) and linear polarization resistance (LPR), are presented in Table 7. The results indicate a measurable reduction in the corrosion current density (*Icorr*) from 1.3418 mA/cm² for the blank solution to 1.0188 mA/cm² for the inhibited solution. This corresponds to a calculated inhibition efficiency of approximately 24 % and a corresponding increase in linear polarization resistance (LPR) from 19.441 to 25.605 Ohm.cm².

Table 7

Parameters of the electrochemical polarization of the medium carbon steel in 0.2 M HCl with and without 500 ppm of the PTF inhibitor

	LPR, Ohm·cm²	Rest Potential, mV	Area, cm²	*Icorr*, mA/cm²	C.R., mmy
BLANK	19.441	-564.31	0.837	1.3418	15.551
500, PPM	25.605	-560.67	0.837	1.0188	11.807

The slight displacement at the anodic and cathodic ends suggests that PTF acts as a mixed-type inhibitor, though its capacity to suppress the metal dissolution and hydrogen evolution reactions is limited at room temperature after prolonged immersion. The classification of PTF as a mixed-type inhibitor in this study is consistent with the observations of Popović, confirming that most pharmaceutical-based green inhibitors suppress both anodic and cathodic reactions simultaneously [38].

3.4 Computational Studies

3.4.1 Molecular Reactivity

Quantum chemical calculations and molecular dynamics simulation were performed to study inhibition properties of PTF molecules on medium carbon steel corrosion. Various quantum chemical parameters including E_{HOMO}, E_{LUMO}, $\Delta E_{(HOMO-LUMO)}$, electronegativity, softness, hardness, electrophilicity, nucleophilicity and electron affinity were discussed to predict the adsorption property as well as inhibition efficiency of the inhibitor molecules. The chemical reactivity of PTF was investigated by means of frontier molecular orbitals HOMO and LUMO [63]. Co-existence of O, N and π-electron system also increases the inhibitor molecules adsorption capacity on the surface of steel.

Figure 9 presents the optimized molecular structures and the HOMO and LUMO density distributions for the PTF inhibitor molecule. Table 9 provides the calculated quantum chemical descriptors, such as energy gap (ΔE), electronegativity (χ), and fraction of electrons transferred (ΔN). Additionally, Table 10 and Figure 11 detail the results of the Monte Carlo simulations, showing the most stable adsorption configurations of PTF on the Fe (110) surface [52 ،53].

The optimized structures of molecules and HOMO and LUMO distributions of the studied inhibitor are presented in Figure 9.

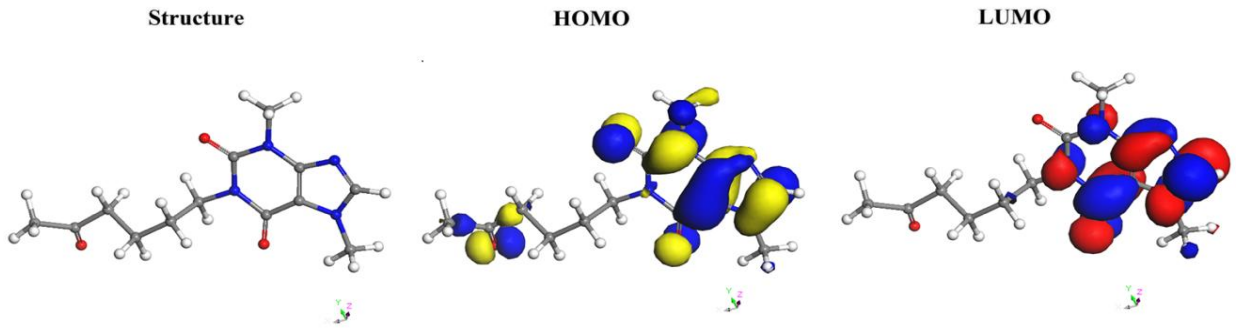

Figure 9. The obtained molecular structure, HOMO and LUMO of the neutral inhibitor molecules using the DFT

Table 8

The net atomic charges of investigated molecule calculated by Mulliken

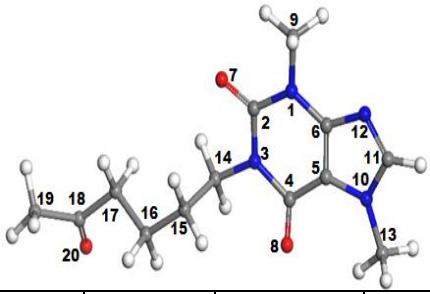

Atom numbering	Mulliken Charge	Atom numbering	Mulliken Charge
N(1)	-0.331	C(11)	-0.057
C(2)	0.558	N(12)	-0.303
N(3)	-0.376	C(13)	0.011
C(4)	0.403	C(14)	-0.082
C(5)	0.126	C(15)	-0.1
C(6)	0.291	C(16)	-0.097
O(7)	-0.499	C(17)	-0.155
O(8)	-0.509	C(18)	0.367
C(9)	0.084	C(19)	-0.208
N(10)	-0.313	O(20)	-0.4

The HOMO density was mainly localized around the oxygen and nitrogen atoms in the PTF molecule and these sites may act as electron donor to the metal surface. On the other hand, the LUMO was pentagonal-shaped and located over two fused heterocyclic π-bond regions. The findings indicate that electron transfer from PTF molecules to the unoccupied *d* orbitals of Fe atoms can be accompanied by a back-donation between the metal surface and the anti-bonding of the inhibitor molecules. Because high electron density, Oxygen and Nitrogen atoms are considered as active adsorption centers. The adsorption active sites of the inhibitor molecules were also identified by Mulliken population analysis. The calculated Mulliken charges of atoms for PTF are listed in Table 8. The identification of nitrogen and oxygen heteroatoms as primary active centers in PTF correlates effectively with the findings of Malki, whose research on quinazolinone derivatives also highlighted these atoms as the key donors for interaction with the iron surface [49].

The result indicated that oxygen atoms, nitrogen atoms and some carbon atoms have negative charge densities, which can provide electrons to the surface of the iron. The atomic charge distribution reveals valuable information on the reactive centres for adsorption. Atoms with higher negative charges can have an enhanced interaction with the empty orbitals of the metal surface [64], this promote the adsorption of inhibitor molecules.

Another critical parameter affecting molecule reactivity and adsorption on metal surfaces is the energy difference between HOMO and LUMO orbitals, ΔE(HOMO-LUMO) [28]. The binding energy was −177.025 eV and the band gap for PTF was 3.477 eV which are given in Table 9. The adsorption of these compounds is also favored by the relatively large negative binding energies which produced stable inhibitor molecules with dominant physical interaction.

Table 9

Calculated quantum chemical parameters for the PTF inhibitor

Theoretical parameters	Value
HOMO, ev	-5.677
LUMO, ev	-2.230
$\Delta E = E_{LUMO} — E_{HOMO}$, eV	3.477
Ionisation, ev	5.677
Affinity, ev	2.23
Electronegativity (χ), eV	3.9535
Hardness (η), ev	1.7385
Softness (σ)	0.5752
Electrons transferred fraction (Δn)	0.87619
Electrophilicity (ω)	4.4953
Binding energy, eV	-177.025

The value of PTFs electronegativity (χ = 3.9535 eV) is also tabulated in Table 9. Electronegativity corresponds to the propensity of molecules to accept that is own electrons [34, 65]. In general, low electronegativity values in metals have been linked to higher inhibition efficacy [66]. The fraction of transferred electrons (ΔN) is also an important quantum quantity. When ΔN is below 3. 6, electrons transfer from the molecule to the metal surface [67]. The computed ΔN value for PTF was 0.87619 eV, suggesting that an electron transfer between inhibitor molecule and steel surface is success and nearly equal to one electron [68].

The electrophylic,ω, can be used as a useful descriptor for molecular reactivity. Species with small electrophilicity values are strong nucleophiles while species with large values of ω are electrophiles. The determined electrophilicity for PTF is 4.4953 eV, which suggest the inhibitor molecule is electrophilic. Moreover, the small magnitude of ionization energy value (I = 5.677 eV) indicates high reactivity of molecule [69], leading to better inhibition efficiency.

Chemical hardness/softness are also useful quantum chemical variables [70]. In general, the smaller the hardness and the higher the softness the better the inhibitors [71]. Calculated value of hardness (η = 1.7385 eV) and softness (σ = 0.5752 eV) of PTF is furnished in Table 9. The bigger hardness with respect to the softness has the physical meaning that the molecule has a rather hard nature.

3.4.2 Monte Carlo Simulation

Molecular dynamics simulation is an excellent modern method to investigate the interaction between inhibitors and metal surface. This study focuses on the use of Monte Carlo simulation to analyse the adsorption of PTF molecules on an Fe (110) surface. In the simulation, a number of key parameters of adsorption are obtained, i.e. the total energy, the adsorption energy, the rigid adsorption energy, and the deformation energy. The parallel orientation of PTF on the Fe(110) surface identified in our Monte Carlo simulations correlates effectively with the configurations reported by Malki for quinazolinone derivatives, proving that such a flat alignment optimizes the interaction of nitrogen and oxygen heteroatoms with the iron lattice [49]. Adsorption energy is the sum of rigid adsorption energy and deformation energy and in the case of adsorption on a steel surface is given in kcal/mol [69, 72, 73]. The adsorption energies for the various adsorption positions of PTF molecules on the Fe (110) surface and with those from Monte Carlo simulation are listed in Table 10. The most stable adsorption configuration is displayed in Figure 10.

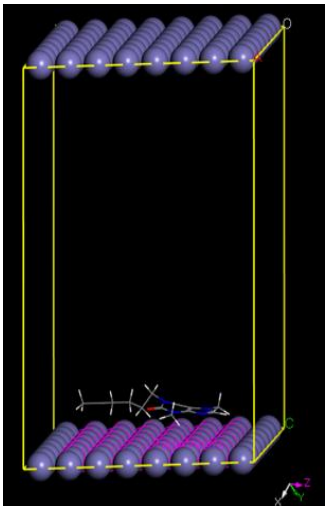

Figure 10. The polymers and descriptors for the lowest adsorption configurations (structure 9) of PTF on the Fe (110) surface obtained by the Monte Carlo simulation.

The parameter (dE_{ads}/dN_i) listed in Table 10 represents the adsorption energy of the steel–adsorbate system after removal of one adsorbate component. The results obtained verify that the chosen adsorption arrangement is the most stable low-energy adsorption configuration for PTF molecules on the surface of Fe (110). The net adsorption energy values were all negative which implied the attraction between inhibitor molecules and the metal is dominated by van der waals forces. In Figure 10, schematic adsorption configurations of single PTF molecules along different directions with the Fe (110) surface are also presented. This Figure shows the most stable equilibrium adsorption structure and the strong interaction between the inhibitor molecules and the metal surface.

Table 10

Outputs and descriptors of the various PTF adsorption configuration structures on Fe (110) calculated by the MC adsorption simulation.

Structures	Total energy, kcal/mol	Adsorption energy, kcal/mol	Rigid adsorption energy, kcal/mol	Deformation energy, kcal/mol	dE_{ad}/d_{Ni}
1	-255.796	-123.463	-128.86	5.399	-123.463
2	-254.715	-122.382	-128.55	6.168	-122.382
3	-254.413	-122.081	-127.522	5.441	-122.081
4	-254.203	-121.87	-127.248	5.378	-121.87
5	-253.928	-121.595	-127.234	5.64	-121.595
6	-253.719	-121.386	-127.2195	5.833	-121.386
7	-253.328	-120.995	-126.679	5.684	-120.995
8	-252.77	-120.437	-125.889	5.452	-120.437
9	-251.428	-119.095	-126.225	7.1296	-119.095

Similarly, in [71] the implication was that planar inhibitor molecules are adsorbed parallel to the metal surface, where electron donation and back-donation, between the inhibitor molecules and metallic surface, dominate the adsorption process [69]. On the other hand, non-planar inhibitor molecules typically exhibit different adsorption behaviour, and for such molecules a straightforward correlation between inhibition efficiency and hardness values can be found.

4 Conclusions

This study establishes pentoxifylline (PTF) as a highly effective and sustainable green corrosion inhibitor for medium carbon steel in 0.2 M HCl, achieving a maximum inhibition efficiency of approximately 90 % at 20 °C and 500 ppm. Experimental investigations reveal that the inhibition mechanism is driven by spontaneous physical adsorption following the Langmuir isotherm, with efficiency decreasing at higher temperatures due to the thermal desorption of the drug film from the steel surface. A significant lesson learned is the potent synergistic effect achieved by combining PTF with iodide ions, which facilitates a more resilient adsorption layer and drastically enhances the protective capacity. These findings are further validated by DFT calculations and Monte Carlo simulations, which identify nitrogen and oxygen heteroatoms as the primary electron-donating centers interacting with the Fe (110) surface. Ultimately, the research confirms that repurposing pharmaceutical molecules offers a non-toxic, cost-effective, and industrially viable strategy for eco-friendly corrosion mitigation.

*Author Information**

**The authors' names are presented in the following order: First Name, Middle Name and Last Name*

Aisha Al-Abbasi (*corresponding author*) — Professor, Candidate of Chemical Sciences, Chemistry Department, Faculty of Science, Sebha University, 071, Sebha, Libya; e-mail: ais.alabbasi@sebhau.edu.ly; https://orcid.org/0000-0002-6082-9246

Hussan Sida — Master Student of Chemical Sciences, Scientific Research Consultation Center, Sebha University, 071, Sebha, Libya; e-mail: hu.sida@sebhau.edu.ly

Hamdy Matter — Associate Professor, Chemistry Department, Faculty of Science, Benghazi University, 061, Benghazi, Libya; e-mail: hamdy.matter@gmail.com, https://orcid.org/0000-0003-3966-566X

Fatima Massoud — Master Student of Chemical Engineering, Chemical Engineering Department, Faculty of Engineering, Sebha University, 071, Sebha, Libya; e-mail: Fati.barka@sebhau.edu.ly

Author Contributions

The manuscript was written through contributions of all authors. All authors have given approval to the final version of the manuscript. CRediT: **Aisha Al-Abbasi:** conceptualization, supervision, methodology, investigation, data curation, validation, writing-original draft, writing-review & editing, and project administration; **Hussan Sida:** investigation, data curation, methodology, visualization, and formal analysis; **Hamdy Matter:** investigation, methodology, and formal analysis related to the electrochemical polarization experiments, as well as interpretation of the electrochemical results; **Fatima Massoud:** investigation and data collection related to the electrochemical polarization experiments.

Acknowledgements

The authors would like to thank the Chemistry Department and Sebha University for providing the laboratory facilities required to carry out this work.

References

1 Al-Abbasi, A. & Sida, H. (2024). Colorimetric evaluation of the corrosion rate of steel in acidic media in the presence of pentoxifylline drug and KI. *Int. J. Corros. Scale Inhib.*, *13*(2), 995-1011. https://doi.org/10.17675/2305-6894-2024-13-2-19

2 Ekeocha, C., Ikenna, O., Etim, I. -I., & Oguzie, E. (2023). Review of forms of corrosion and mitigation techniques: A visual guide. *African Scientific Reports*, 117. https://doi.org/10.46481/asr.2023.2.3.117

3 Al-abbasi, A., Zirik, R., Ahwidi, H., & Massoud, F. (2025). Corrosion Mitigation of Medium Carbon Steel in HCl Solution Using Ficus Carica Leaf Extract: Mass Loss Technique. *Journal of Pure & Applied Sciences 24*(3), 105-109. https://doi.org/10.51984/jopas.v24i3.4199

4 Kumar, N., Anunay, P., Kumar, S., Meena, L. K., & Singh, D. (2026). An overview on emerging green organic corrosion inhibitors: sustainable solution for oil and gas industrial applications. *RSC Advances*, *16*(5), 3909-3948. https://doi.org/10.1039/D5RA08166A

5 Abbas, A., Adesina, A. Y., & Suleiman, R. K. (2023). Influence of Organic Acids and Related Organic Compounds on Corrosion Behavior of Stainless Steel—A Critical Review. Metals, 13(8), 1479. https://doi.org/10.3390/met13081479

6 Dalmora, G. P. V., Borges Filho, E. P., Maraschin Conterato, A. A., Roso, W. S., Pereira, C. E., & Dettmer, A. (2025). Methods of corrosion prevention for steel in marine environments: A review. *Results in Surfaces and Interfaces*, *18*, 100430. https://doi.org/https://doi.org/10.1016/j.rsurfi.2025.100430

7 Khaled, K. F. & Hackerman, N. (2003). Investigation of the inhibitive effect of ortho-substituted anilines on corrosion of iron in 1 M HCl solutions. *Electrochimica Acta*, *48*(19), 2715-2723. https://doi.org/http://dx.doi.org/10.1016/S0013-4686(03)00318-9

8 Bahrami, M. J., Hosseini, S. M. A., & Pilvar, P. (2010). Experimental and theoretical investigation of organic compounds as inhibitors for mild steel corrosion in sulfuric acid medium. *Corros Sci*, *52*. https://doi.org/10.1016/j.corsci.2010.04.024

9 Goulart, C. M., Esteves-Souza, A., Martinez-Huitle, C. A., Rodrigues, C. J. F., Maciel, M. A. M., & Echevarria, A. (2012). Experimental and theoretical evaluation of semicarbazones and thiosemicarbazones as organic corrosion inhibitors. *Corrosion Science*, *67*, 281-291. https://doi.org/http://dx.doi.org/10.1016/j.corsci.2012.10.029

10 Suliman, M. S., & Al-abbasi, A. (2007). The synergistic effect of halide ions and organic nitrogen containing compounds on the inhibition of mild steel corrosion in hydrochloric acid solution. In *Proceedings of the 6th Libyan Corrosion Conference* (Vol. 6). Tripoli, Libya

11 Yadav, M., Kumar, S., Sinha, R. R., Bahadur, I., & Ebenso, E. E. (2015). New pyrimidine derivatives as efficient organic inhibitors on mild steel corrosion in acidic medium: Electrochemical, SEM, EDX, AFM and DFT studies. *Journal of Molecular Liquids*, *211*, 135-145. http://dx.doi.org/10.1016/j.molliq.2015.06.063

12 Al-abbasi, A. A., Mohamed Tahir, M. I., & Kassim, M. B. (2012). N-(Pyrrolidin-1-ylcarbothioyl)benzamide. *Acta Crystallographica Section E*, *68*(1), o201. https://doi.org/doi:10.1107/S1600536811053694

13 Al-abbasi, A. & Kassim, M. (2011). 1-Ethyl-1-methyl-3-(2-nitrobenzoyl)thiourea. *Acta Crystallographica Section E*, *67*(7), o1840. https://doi.org/doi:10.1107/S1600536811024652

14 Al-abbasi, A., Tan, S., & Kassim, M. (2010). 1-Benzoyl-3-(4-hydroxyphenyl)thiourea. *Acta Crystallographica Section E*, *66*(12), o3181. https://doi.org/doi:10.1107/S1600536810045988

15 Belkher, N. A., Al-abbas, A.A., & Zidan, M. (2019). Potentiometric Studies on Stability Constant of the Complexes of SomeEssential Transition Metal Ions with L-Valine. *Journal of Pure & Applied Science 13*(3), 59-63. https://doi.org/10.51984/jopas.v18i3.240

16 Al-abbasi, A., and Shana, I. (2021). Corrosion Inhibition of Mild Steel in Acidic Media by Expired Carbimazole Drug. *Journal of Pure & Applied Sciences*, *20*(2), 176–180. https://doi.org/10.51984/jopas.v20i2.1646

17 AL-abbassi, A., Taher, G., Matrood, E., Dnkm, A., Sallh, A., Izrik, R., & Suliman, M. (2020). Study of the Behavior of Sodium Diclofenac Expired Drug as an Corrosion Inhibitor of Iron in Sulfuric Acid Using UV-VIS Spectrophotometry. International Journal of Scientific Research in Science, Engineering and Technology, 233–242. Internet Archive. https://doi.org/10.32628/ijsrset207248

18 Khalifa, S., AL-abbassi, A., Suliman, M. (2018). Adsorption and Corrosion Inhibition of Mild Steel in Acidic Media by Expired Pharmaceutical Drug. *Journal of Pure & Applied Sciences*, *17*, 1-6. https://doi.org/10.51984/jopas.v17i4.414

19 Al-abbasi, A., Alqasim, Z. A., Rahuma, F., & Mona, H. (2024). Corrosion Inhibition of Reinforced Steel in 3.5 % Sodium Chloride using Expired Pentoxifylline Drug: A Mass Loss Study. *International Science and Technology Journal*, *2*, 1-21. https://doi.org/www.doi.org/10.62341/ISTJ

20 Gece, G. k. (2011). Drugs: A review of promising novel corrosion inhibitors. *Corrosion Science*, *53*(12), 3873-3898. https://doi.org/http://dx.doi.org/10.1016/j.corsci.2011.08.006

21 Njoku, C. N., Maduoma, T. U., Emori, W., Odey, R. E., Unimke, B. M., Yakubu, E., Anorondu, C. C., Udunwa, D. I., Njoku, O. C., & Oyoh, K. B. (2023). Natural and synthetic drugs as eco-friendly and sustainable corrosion inhibitors for metals: a review. Pigment &Amp; Resin Technology, 53(6), 1074–1087. https://doi.org/10.1108/prt-07-2023-0063

22 AL-Abbasi, A. (2006). *Study of corrosion inhibition kinetics of steel by using some organic compounds* [Master's thesis, Sebha University. Sebha University Repository.

23 Al-abbasi, A. S. M., & Milad, A. (2017). The synergistic effects of iodide ions on the corrosion inhibition of mild steel in H2SO4 using phenyl benzoylthiourea. In *Proceedings of the 1st International Conference on Science and Technology*. Sebha, Libya

24 Hazazi, O. A., & Abdallah, M. (2013). Prazole Compounds as Inhibitors for Corrosion of Aluminum in Hydrochloric acid. International Journal of Electrochemical Science, 8(6), 8138–8152. https://doi.org/10.1016/s1452-3981(23)12874-4

25 Elsaeed, S. M., El Tamany, E. S. H., Ashour, H., Zaki, E. G., Khamis, E. A., & El Nagy, H. A. (2018). Corrosion and hydrogen evolution rate control for X-65 carbon steel based on chitosan polymeric ionic liquids: experimental and quantum chemical studies. *RSC Advances*, *8*(66), 37891-37904. https://doi.org/10.1039/C8RA05444D

26 Becke, A. D. (1988). Density-functional exchange-energy approximation with correct asymptotic behavior. Physical Review A, 38(6), 3098–3100. https://doi.org/10.1103/physreva.38.3098

27 Lee, C., Yang, W., & Parr, R. G. (1988). Development of the Colle-Salvetti correlation-energy formula into a functional of the electron density. *Physical Review B, 37*(2), 785. https://doi.org/10.1103/physrevb.37.785

28 Kara, Y. S., Sagdinc, S. G., & Esme, A. (2012). Theoretical study on the relationship between the molecular structure and corrosion inhibition efficiency of long alkyl side chain acetamide and isoxazolidine derivatives. *Protection of Metals and Physical Chemistry of Surfaces*, *48*(6), 710-721. https://doi.org/10.1134/s2070205112060056

29 Sastri, V. S. & Perumareddi, J. R. (1994). Selection of Corrosion Inhibitors for Use in Sour Media. *CORROSION*, *50*(6), 432-437. https://doi.org/doi:10.5006/1.3293521

30 Pearson, R. G. (1988). Absolute electronegativity and hardness: application to inorganic chemistry. *Inorganic Chemistry*, *27*(4), 734-740. https://doi.org/10.1021/ic00277a030

31 Martinez, S. (2003). Inhibitory mechanism of mimosa tannin using molecular modeling and substitutional adsorption isotherms. *Materials Chemistry and Physics*, *77*(1), 97-102. http://dx.doi.org/10.1016/S0254-0584(01)00569-7

32 Khalil, N. (2003). Quantum chemical approach of corrosion inhibition. *Electrochim Acta*, *48*. https://doi.org/10.1016/s0013-4686(03)00307-4

33 Gece, G. (2008). The use of quantum chemical methods in corrosion inhibitor studies. *Corros Sci*, *50*. https://doi.org/10.1016/j.corsci.2008.08.043

34 Parr, R. G., Szentpály, L. V., & Liu, S. (1999). Electrophilicity index. *Journal of the American Chemical Society*, *121*(9), 1922-1924.

35 Khaled, K. F. & El-Maghraby, A. (2010). Experimental, Monte Carlo and molecular dynamics simulations to investigate corrosion inhibition of mild steel in hydrochloric acid solutions. *Arabian Journal of Chemistry*, *7*(3), 319-326. http://dx.doi.org/10.1016/j.arabjc.2010.11.005

36 Musa, A. Y., Jalgham, R. T. T., & Mohamad, A. B. (2011). Molecular dynamic and quantum chemical calculations for phthalazine derivatives as corrosion inhibitors of mild steel in 1 M HCl. *Corrosion Science*, *56*, 176-183. http://dx.doi.org/10.1016/j.corsci.2011.12.005

37 Akinbulumo, O. A., Odejobi, O. J., & Odekanle, E. L. (2020). Thermodynamics and adsorption study of the corrosion inhibition of mild steel by Euphorbia heterophylla L. extract in 1.5 M HCl. *Results in Materials*, *5*, 100074. https://doi.org/10.1016/j.rinma.2020.100074

38 Popović, A. S., Aligayev, A., Trajković, D. V., Jovanović, G., Rakočević, L., & Grgur, B. N. (2026). Coupled experimental and theoretical investigation of an antidiabetic drug as a green corrosion inhibitor for low-carbon steel in acidic media. *Journal of Electroanalytical Chemistry*, *1011*, 120076. https://doi.org/10.1016/j.jelechem.2026.120076

39 Abdul Rahiman, A. F. S. & Sethumanickam, S. (2017). Corrosion inhibition, adsorption and thermodynamic properties of poly(vinyl alcohol-cysteine) in molar HCl. *Arabian Journal of Chemistry*, *10*, S3358-S3366. https://doi.org/10.1016/j.arabjc.2014.01.016

40 Mahmood, A. *et al.* (2025). Corrosion inhibition of steel in acidic solution using p-bromopiperazinylbenzene: Experimental and DFT calculations. *International Journal of Corrosion and Scale Inhibition*, *14*, 706-729. https://doi.org/10.17675/2305-6894-2025-14-2-15

41 Kumar Shukla S., Tanwer, S. (2021). Evaluation of Corrosion inhibition properties of pharmaceutically active compound Cefotaxime sodium on mild steel surface in sulfuric acid medium. Journal of the Turkish Chemical Society Section A: Chemistry, 8(4), 1099–1110. https://doi.org/10.18596/jotcsa.972325

42 Umoren, S. A., Solomon, M. M., Udosoro, I. I., & Udoh, A. P. (2010). Synergistic and antagonistic effects between halide ions and carboxymethyl cellulose for the corrosion inhibition of mild steel in sulphuric acid solution. *Cellulose*, *17*(3), 635-648. https://doi.org/10.1007/s10570-010-9409-7

43 Schorr, M., & Yahalom, J. (1972). The significance of the energy of activation for the dissolution reaction of metal in acids. Corrosion Science, 12(11), 867–868. https://doi.org/10.1016/s0010-938x(72)80015-5

44 Ebenso, E. E., & Obot, I. B. (2010). Inhibitive Properties, Thermodynamic Characterization and Quantum Chemical Studies of Secnidazole on Mild Steel Corrosion in Acidic Medium. International Journal of Electrochemical Science, 5(12), 2012–2035. https://doi.org/10.1016/s1452-3981(23)15402-2

45 Ebenso, E. E. (2003). Synergistic effect of halide ions on the corrosion inhibition of aluminium in H2SO4 using 2-acetylphenothiazine. *Materials Chemistry and Physics*, *79*(1), 58-70. https://doi.org/10.1016/S0254-0584(02)00446-7

46 Deyab, M. A., & El-Rehim, S. S. A. (2014). Effect of succinic acid on carbon steel corrosion in produced water of crude oil. Journal of the Taiwan Institute of Chemical Engineers, 45(3), 1065–1072. https://doi.org/10.1016/j.jtice.2013.09.004

47 Deyab, M. A. (2015). Egyptian licorice extract as a green corrosion inhibitor for copper in hydrochloric acid solution. Journal of Industrial and Engineering Chemistry, 22, 384–389. https://doi.org/10.1016/j.jiec.2014.07.036

48 Obot, B., Obi-Egbedi, N. O., & Umoren, S. A. (2009). Experimental and theoretical investigation of clotrimazole as corrosion inhibitor for aluminium in hydrochloric acid and effect of iodide ion addition. *Der Pharma Chemica*, *1*(1), 151-166.

49 Hashim, N. M., Rahim, A. A., Osman, H., & Raja, P. B. (2012). Quinazolinone compounds as corrosion inhibitors for mild steel in sulfuric acid medium. Chemical Engineering Communications, 199(6), 751–766. https://doi.org/10.1080/00986445.2011.617801

50 Abdel Hameed, R., Essa, A., Mohamed, D., Abdallah, M., Aljohani, M., Al-Mhyawi, S., Soluman, M., & Arafa, E. (2021). Evaluation of Expired Augmentine Drugs as Corrosion Inhiitor for Carbon Steel Alloy in 1.0 n hcl Acidic Environment Using Analytical Techniques. *Egyptian Journal of Chemistry*, *65*(4), 735-745. https://doi.org/10.21608/ejchem.2021.95853.4495

51 Feng, L., Zhang, S., Zhou, Y., Pan, R., Du, H., Liu, F., & Yang, Y. (2023). Expired Glucosamine Drugs as Green Corrosion Inhibitors for Carbon Steel in H2SO4 Solution and Synergistic Effect of Glucosamine Molecules with Iodide Ions: Combined Experimental and Theoretical Investigations. *Crystals*, 13(2), 205. https://doi.org/10.3390/cryst13020205

52 Kur'yato, L. E. T. a. V. A. (2025). Anticorrosive, antihydrogenating and bactericidal effects of a number of expired drugs. *International Journal of Corrosion and Scale Inhibition*, 14(4). https://doi.org/10.17675/2305-6894-2025-14-4-6

53 Wang, X., Yang, H., & Wang, F. (2011). An investigation of benzimidazole derivative as corrosion inhibitor for mild steel in different concentration HCl solutions. *Corrosion Science*, *53*(1), 113-121. https://doi.org/10.1016/j.corsci.2010.09.029

54 Zhang, H. -h., Gao, K., Yan, L., & Pang, X. (2017). Inhibition of the corrosion of X70 and Q235 steel in CO2-saturated brine by imidazoline-based inhibitor. *Journal of Electroanalytical Chemistry*, *791*, 83-94. https://doi.org/10.1016/j.jelechem.2017.02.046

55 Zheng, T., Liu, J., Wang, M., Liu, Q., Wang, J., Chong, Y., & Jia, G. (2022). Synergistic corrosion inhibition effects of quaternary ammonium salt cationic surfactants and thiourea on Q235 steel in sulfuric acid: Experimental and theoretical research. Corrosion Science, 199, 110199. https://doi.org/10.1016/j.corsci.2022.110199

56 Ali, S. M. & Al Lehaibi, H. A. (2016). Control of zinc corrosion in acidic media: Green fenugreek inhibitor. *Transactions of Nonferrous Metals Society of China*, *26*(11), 3034-3045. https://doi.org/10.1016/S1003-6326(16)64434-5

57 Mohamed, K. E. M., Ibrahim, O. H., El-Bedawy, M. E., & Ali, A. H. (2020). Synergistic effect of different Zn salts with sodium octanoate on the corrosion inhibition of carbon steel in cooling water. *Journal of Radiation Research and Applied Sciences*, *13*(1), 276-287. https://doi.org/10.1080/16878507.2020.1730603

58 Khadom, A. A., Abd, A. N., & Ahmed, N. A. (2022). Synergistic effect of iodide ions on the corrosion inhibition of mild steel in 1 M HCl by Cardaria Draba leaf extract. *Results in Chemistry*, *4*, 100668. https://doi.org/10.1016/j.rechem.2022.100668

59 Tang, M., Li, X., Deng, S., & Lei, R. (2021). Synergistic inhibition effect of Mikania micrantha extract with KI on steel corrosion in H2SO4 solution. *Journal of Molecular Liquids*, *344*, 117926. https://doi.org/10.1016/j.molliq.2021.117926

60 Oza, B. N., Sinha, R.S. (1982). Thermometric study of corrosion behaviour of high strength Al–Mg alloy in phosphoric acid in presence of halides. *Trans SAEST*, *17*(1), 281–285.

61 El-Awady, A. A., Abd-El-Nabey, B. A., & Aziz, S. G. (1992). Kinetic-Thermodynamic and Adsorption Isotherms Analyses for the Inhibition of the Acid Corrosion of Steel by Cyclic and Open-Chain Amines. Journal of the Electrochemical Society, 139(8), 2149–2154. https://doi.org/10.1149/1.2221193

62 Ituen, E., Akaranta, O., & James, A. (2017). Evaluation of Performance of Corrosion Inhibitors Using Adsorption Isotherm Models: An Overview. *Chemical Science International Journal*, *18*, 1-34. https://doi.org/10.9734/CSJI/2017/28976

63 Madkour, L. H. & Elshamy, I. H. (2016). Experimental and computational studies on the inhibition performances of benzimidazole and its derivatives for the corrosion of copper in nitric acid. *International Journal of Industrial Chemistry*, *7*(2), 195-221. https://doi.org/10.1007/s40090-015-0070-8

64 Yang, W. & Parr, R. G. (1985). Hardness, softness, and the fukui function in the electronic theory of metals and catalysis. *Proc Natl Acad Sci U S A*, *82*(20), 6723-6. https://doi.org/10.1073/pnas.82.20.6723

65 Chattaraj, P. K., Sarkar, U., & Roy, D. R. (2006). Electrophilicity Index. *Chemical Reviews*, *106*(6), 2065-2091. https://doi.org/10.1021/cr040109f

66 Zarrouk, A., Hammouti, B., Dafali, A., Bouachrine, M., Zarrok, H., Boukhris, S., & Al-Deyab, S. S. (2014). A theoretical study on the inhibition efficiencies of some quinoxalines as corrosion inhibitors of copper in nitric acid. *Journal of Saudi Chemical Society*, 18(5), 450–455. https://doi.org/10.1016/j.jscs.2011.09.011

67 Martinez, S., & Štagljar, I. (2003). Correlation between the molecular structure and the corrosion inhibition efficiency of chestnut tannin in acidic solutions. *Journal of Molecular Structure: THEOCHEM*, 640(1-3), 167–174. http://dx.doi.org/10.1016/j.theochem.2003.08.126

68 Lukovits, I., Kálmán, E., & Pálinkás, G. (1995). Nonlinear Group-Contribution Models of Corrosion Inhibition. *Corrosion*, 51(3), 201–205. https://doi.org/10.5006/1.3294362

69 Khaled, K. F. (2009). Experimental and atomistic simulation studies of corrosion inhibition of copper by a new benzotriazole derivative in acid medium. *Electrochimica Acta*, *54*(18), 4345-4352. http://dx.doi.org/10.1016/j.electacta.2009.03.002

70 Kaya, S. & Kaya, C. (2015). A new method for calculation of molecular hardness: A theoretical study. *Computational and Theoretical Chemistry*, *1060*, 66-70. https://doi.org/10.1016/j.comptc.2015.03.004

71 Ebenso, E. E., Isabirye, D. A., & Eddy, N. O. (2010). Adsorption and quantum chemical studies on the inhibition potentials of some thiosemicarbazides for the corrosion of mild steel in acidic medium. *Int J Mol Sci*, *11*. https://doi.org/10.3390/ijms11062473

72 Zeng, J., Zhang, J., & Gong, X. Molecular dynamics simulation of interaction between benzotriazoles and cuprous oxide crystal. *Computational and Theoretical Chemistry*, *963*(1), 110-114. http://dx.doi.org/10.1016/j.comptc.2010.10.006

73 Znini, M., Majidi, L., Bouyanzer, A., Paolini, J., Desjobert, J.M., & Costa, J., Hammouti, B. (2012). Essential oil of Salvia aucheri mesatlantica as a green inhibitor for the corrosion of steel in 0.5 M H2SO4. *Arabian Journal of Chemistry*, *5*(4), 467-474. https://doi.org/10.1016/j.arabjc.2010.09.017